Journal of Power Sources 237 (2013) 5–12

Contents lists available at SciVerse ScienceDirect

Journal of Power Sources

journal homepage: www.elsevier.com/locate/jpowsour

Bicyclic imidazolium ionic liquids as potential electrolytes for rechargeable lithium ion batteries

Xiao-Guang Sun [a,*], Chen Liao [a], Nan Shao [a], Jason R. Bell [b], Bingkun Guo [a], Huimin Luo [b], De-en Jiang [a], Sheng Dai [a,c,**]

[a] Chemical Science Division, Oak Ridge National Laboratory, Oak Ridge, TN 37831-6201, USA
[b] Energy and Transportation Science Division, Oak Ridge National Laboratory, Oak Ridge, TN 37831-6181, USA
[c] Department of Chemistry, University of Tennessee, Knoxville, TN 37996, USA

HIGHLIGHTS

- First report using bicyclic imidazolium ionic liquid as electrolyte for lithium ion battery.
- Bicyclic imidazolium ionic liquid shows good SEI formation ability on graphite electrode surface.
- Bicyclic imidazolium ionic liquid is compatible with graphite electrode without using additives.
- Good cycling stability is achieved at 50 °C because of lower charge transfer impedance.

ARTICLE INFO

Article history:
Received 29 September 2012
Received in revised form
30 January 2013
Accepted 22 February 2013
Available online 1 March 2013

Keywords:
Lithium ion battery
1-Ethyl-2,3-trimethyleneimidazolium bis(trifluoromethane sulfonyl)imide ([ETMIm][TFSI])
Solid electrolyte interphase (SEI)
Impedance spectroscopy

ABSTRACT

A bicyclic imidazolium ionic liquids, 1-ethyl-2,3-trimethyleneimidazolium bis(tri fluoromethane sulfonyl) imide ([ETMIm][TFSI]), and reference imidazolium compounds, 1-ethyl-3-methylimidazolium bis(trifluoromethane sulfonyl)imide ([EMIm][TFSI]) and 1, 2-dimethyl-3-butylimidazolium bis(trifluoromethane sulfonyl)imide ([DMBIm][TFSI]), were synthesized and investigated as solvents for lithium ion batteries. Although the alkylation at the C-2 position of the imidazolium ring does not affect the thermal stability of the ionic liquids, the stereochemical structure of the molecules has shown profound influences on the electrochemical properties of the corresponding ionic liquids. [ETMIm][TFSI] has better reduction stability than both [EMIm][TFSI] and [DMBIm][TFSI], as confirmed by both linear sweep voltammetry (LSV) and theoretical calculation. Also, a relatively stable solid electrolyte interphase (SEI) is formed in [ETMIm][TFSI], suggested by the time dependence of the impedance spectra of the Li||Li cell. Furthermore, the Li||graphite half-cell based on [BTMIm][TFSI] exhibits reversible capacity of 250 mA h g^{-1} and 70 mA h g^{-1} at 25 °C, which increases to 330 mA h g^{-1} and 250 mA h g^{-1} at 50 °C, under the current rate of C/20 and C/10, respectively. For comparison, the half-cell based on [DMBIm][TFSI] exhibits poor capacity retention under the same current rates at both temperatures.

Published by Elsevier B.V.

1. Introduction

Conventional lithium ion battery electrolytes are composed of a mixture of volatile cyclic and linear carbonates such as ethylene carbonate (EC), dimethyl carbonate (DMC), ethyl methyl carbonate (EMC), diethyl carbonate (DEC), and so on, which present a safety concern for large lithium ion batteries that have been proposed for electric vehicle applications. As an alternative, ionic liquids (ILs), which are semi-organic salts, offer several unique safe electrolyte properties such as little or no vapor pressure, excellent chemical and thermal stability, and most important, a wide electrochemical window. Therefore, in the last few years IL-based electrolytes have been actively studied for applications in lithium ion batteries [1–25].

Among different ILs studied, 1,3-dialkylimidazolium bis(trifluoromethane sulfonyl)imide remains a favorite because of its typical low viscosity and high ionic conductivity [10,15,16,21,23]. However, the activity of the hydrogen atom on the C-2 position of the imidazolium ring results in a relatively high reduction potential of 1.0 V versus Li/Li^+, which is too positive to allow lithium

* Corresponding author. Tel.: +1 865 241 8822.
** Corresponding author. Department of Chemistry, University of Tennessee, Knoxville, TN 37996, USA. Tel.: +1 865 574 5033.
E-mail addresses: sunx@ornl.gov (X.-G. Sun), dais@ornl.gov (S. Dai).

0378-7753/$ – see front matter Published by Elsevier B.V.
http://dx.doi.org/10.1016/j.jpowsour.2013.02.061

deposition or intercalation and thus not suitable for application in lithium ion batteries. Seki et al. showed that the cycling stability and coulombic efficiency of the $LiCoO_2$||Li cells were improved when the acidic proton in the C-2 position of the imidazolium ring was replaced by a methyl group [26]. It was also shown that even the hydrogen of the methyl group at the C-2 position of the imidazolium ring could be easily deprotonated by a strong base such as butyllithium [27]. To further improve the stability of the imidazolium ring, Chu et al. attached a longer alkyl chain at the C-2 position, which formed a stable bicyclic imidazolium structure [28,29]. Unfortunately, so far there are no reports on the use of bicyclic imidazolium ILs for lithium ion battery applications. In fact, it might be advantageous to use bicyclic imidazolium ILs for lithium ion batteries, considering their unique stereochemistry. It has been reported that the noncyclic dialkylimidazolium cation could be easily co-intercalated into the graphite electrode, either with or without a companion lithium cation, through the adaption of a single plane orientation [19,30]. Because of its intrinsic stereochemistry, the cyclic alkane ring of the bicyclic imidazolium cation is not in the same plane as the imidazolium ring; therefore, it is expected that the bicyclic imidazolium cation should not be easily co-intercalated into the graphite electrode during the lithium intercalation process. This favorable property inspires us to evaluate the physical and electrochemical properties of bicyclic imidazolium ILs for applications in lithium ion batteries.

2. Experimental

2.1. Synthesis

Lithium foil, carbon black, polyvinylvinylidifluoride, *N*-methylpyrrolidinole (NMP), and charcoal were all obtained from Aldrich and were used as supplied. Lithium bis(trifluoromethanesulfonyl) imide (LiTFSI) (purity, 99.5%) was obtained from 3 M. Natural graphite was obtained from Pred Materials. Carbon black and copper foil (25 μm) were purchased from MTI Corporation. Deionized H_2O was obtained via the use of a Millipore ion-exchange resin deionizer. Celgard 3401 was obtained from Celgard as an evaluation sample.

A typical bicyclic imidazolium IL, 1-ethyl-2,3-trimethyleneimidazolium bis(trifluoromethanesulfonyl)imide ([ETMIm][TFSI]), was synthesized by a modified literature method (Scheme 1) [28,29]. For comparison, the ILs 1-ethyl-3-methylimidazolium bis(trifluoro methanesulfonyl)imide ([EMIm][TFSI]), and 1-butyl-2,3-dimethylimidazolium bis(trifluoromethane sulfonyl)imide ([DMBIm][TFSI]) were also synthesized according to the reference (Scheme 1) [1]. The ILs were dried by freeze drying for four days under vacuum at room temperature and then stored over freshly activated 4A molecular sieves in an argon-filled glovebox. The water content was less than 50 ppm as detected by Karl-Fisher's titration.

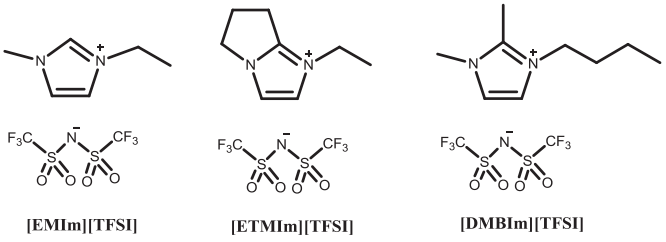

Scheme 1. Structures of ionic liquids.

LiTFSI was dried at 140 °C under high vacuum for 48 h. The 0.5 M LiTFSI electrolyte solutions were prepared by dissolving a calculated amount of LiTFSI in the ILs under heat inside a glovebox.

2.2. Characterization

The thermal properties of ILs and their salt solutions were determined by using thermal gravimetric analysis (TGA TA 2950) and differential scanning calorimetry (DSC Q100). The TGA measurement was carried out at a scan rate of 10 °C min^{-1} from room temperature to 800 °C under a nitrogen atmosphere. The glass transition (onset point) and melting point (peak position) were obtained under a scan rate of 10 °C min^{-1} in the temperature range of from −90 to 100 °C.

The reduction potential of the pure ILs was measured using cyclic voltammetry on a Gamry instrument at ambient temperature. A self-made three-electrode cell with glass-sealed platinum wire as working, counter, and reference electrode, respectively. The potential was calibrated using the redox potential of a ferrocene/ferrocenium (Fc/Fc^+) couple measured in each IL.

A graphite electrode was obtained by casting a well-homogenized slurry of graphite (90 wt%) and PVdF (10 wt%) in NMP on copper foil using a doctor blade. After the solvent was evaporated, the electrodes were pressed under a hydrolytic pressure of 1 Ton for 1 min before being cut into discs with a diameter of 13 mm and further dried at 110 °C for 24 h. They were then transferred into a glovebox for cell assembly. The coin cell was assembled with graphite as the cathode, lithium foil as the anode, and 0.5 M LiTFSI/IL as the electrolyte. Celgard 3401 was used as the separator.

Viscosity measurement was performed with a Brookfield model DV-II PRO Viscometer. The dried ionic liquid or its salt solution was loaded into the sample chamber and maintained at 25 °C for 10 min to ensure thermal equilibrium before the measurement was obtained.

The ionic conductivity of the IL electrolyte, as well as the impedance of the Li||Li cells, was measured by ac impedance spectroscopy using a Gamry instrument in the frequency range from 3×10^5 Hz to 1 Hz with a perturbation amplitude of 10 mV. The conductivity measurement was carried out in a conductivity cell, made in-house, with two parallel glass-sealed platinum electrodes. The cell was placed in an aluminum block that was heated from room temperature to 100 °C, with equilibration time of 30 min at each measuring temperature. The cell constants were calibrated with a 0.1 M KCl aqueous standard solution at 25 °C.

Theoretical calculations were employed to compute the reduction potentials of the imidazolium cations using the same method reported earlier [31]. Possible conformers of the imidazolium cations were optimized at the B3LYP/6-31 + G(d,p) level [32,33] and compared in stability. Reduction potentials were then obtained for the lowest energetic conformers by using a thermodynamic cycle and the polarizable continuum model of solvation [34,35]. All calculations were done by GAUSSIAN09 software [36].

3. Results and discussion

3.1. Thermal properties

The thermal stabilities of the ILs, with and without LiTFSI, were tested under nitrogen atmosphere between room temperature and 800 °C at a heating rate of 10 °C min^{-1}. As shown in Fig. 1, the three pure ILs have similar thermal stabilities, which are well above 450 °C. This is not surprising considering they all have the same core structure, the imidazole ring, even though they have different chain length substituents. In addition, the decomposition

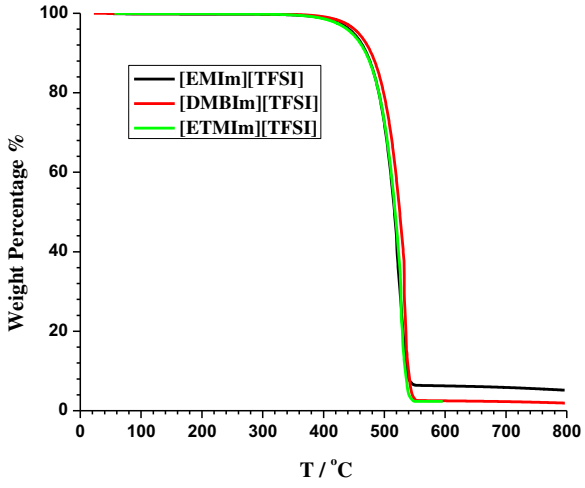

Fig. 1. TGA Trace of pure ionic liquids.

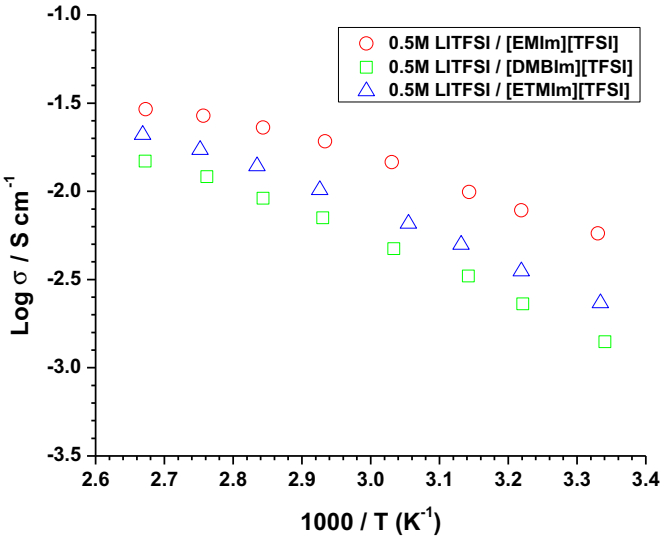

Fig. 2. The temperature dependence of the ionic conductivities of ionic liquids containing 0.5 M LiTFSI.

temperatures of the ILs with 0.5 M LiTFSI are almost the same as those of pure ILs (not shown), which is similar to that observed for pyrrolidinium based ionic liquids [37,38].

Table 1 summarizes the thermal properties measured by DSC. For the reference IL [EMIm][TFSI], the melting point (T_m) of −12.0 °C is in agreement with the results reported in the literature. [4] However, because the low-temperature limit of the DSC Q100 is −90.0 °C, the glass transition temperature (T_g) of [EMIm][TFSI] cannot be detected. [4] For the same reason, neither the T_g of pure [ETMIm][TFSI] nor that of the solution of 0.5 M LiTFSI/[EMIm][TFSI] can be observed using Q100. It is generally observed that for the pure ILs, the T_g is primarily determined by the viscosity of the IL [39], whereas T_m is determined by the symmetry of the cation. For example, the T_g increases on the order of [EMIm][TFSI] < [ETMIm][TFSI] < [DMBIm][TFSI], following the order of increasing viscosity (molecular weight) of the ILs (Table 1), whereas the melting point decreases in the order of [ETMIm][TFSI] > [EMIm][TFSI] > [DMBIm][TFSI], following the order of enhancing asymmetry of the cations. It is also observed that the T_g of the IL salt solution (0.5 M LiTFSI) is always higher than that of the pure IL, which is solely due to the increased viscosity of the salt solution versus that of pure IL (Table 1).

3.2. Ionic conductivity

Fig. 2 shows the ionic conductivity of the ILs with 0.5 M LiTFSI, which can be described by the Vogel–Fulcher–Tamman (VFT) equation:

$$\sigma = \sigma_0 \exp[-B/(T - T_0)] \quad (1)$$

where σ_0 (K S cm^{-1}) is a constant, B (K) is the pseudo-activation energy, and T_0 (K) is the vanishing ion mobility temperature. The parameters for σ_0, B, and T_0 were obtained by best fitting the conductivity data in Fig. 2 using Eq. (1) and are summarized in Table 2. At room temperature, the ionic conductivities of the IL electrolytes follow the order of EMIm > ETMIm > DMBIm, which is consistent with the viscosity data in Table 1, that is, the larger the cation, the more viscous is the ionic liquid and its solution and thus the lower is the ionic conductivity. It is noted that the pseudo-activation energies of ILs with C-2 acidic protons are much smaller than those of ILs with C-2 alkyl groups (Table 2), indicating the advantages of the former in terms of ion mobility.

3.3. Electrochemical properties

Fig. 3 shows the linear sweep voltammograms of the pure ILs scanned from 0.5 V to −3.0 V under a scan rate of 10 mV s^{-1} at room temperature. The cathodic reduction potential ($E_{cathodic}$) extrapolated from Fig. 3 shows the following reduction stability: [EMIm][TFSI] << [DMBIm][TFSI] < [ETMIm][TFSI], which is consistent with that reported by Sekei et al. on the enhanced reduction stability of dimethylalkylimidazolium ILs compared with that of methylalkylimidazolium ILs [26].

To understand the trend of the reduction potentials for the synthesized ILs, quantum mechanical calculations were also performed using the method reported earlier [31]. For an IL electrolyte, the lowest unoccupied molecular orbital (LUMO) is localized on the cation that will receive the electron. The calculated LUMO level of the three ILs, along with the calculated reduction potentials against

Table 1
Thermal properties of synthesized ILs and their 0.5 M LiTFSI salt solutions.

Ionic liquids	T_g/°C[a]	T_c/°C[b]	T_m/°C[c]	η/cp[d]
[EMIm][TFSI]	−87.0[e]	−28.0	−12.0	31.5
0.5°cm LiTFSI/[EMIm][TFSI]	–	−32.5	−20.0	46.0
[DMBIm][TFSI]	−76.0	–	–	97.5
0.5°cm LiTFSI/[DMBIm][TFSI]	−72.0	–	–	159.7
[ETMIm][TFSI]	–	−16.0	27.5	83.4
0.5°cm LiTFSI/[ETMIm][TFSI]	−78.0	−26.5	21.0	142.5

[a] Onset temperature of a heat capacity change (T_g).
[b] Crystallization temperature defined by the exothermic peak (T_c) measured by DSC.
[c] Melting temperature defined by the endothermic peak (T_m) measured by DSC.
[d] Viscosity measured at 25 °C.
[e] From J. Phys. Chem. B., 110 (2006) 19593–19600.

Table 2
VFT fitting parameters of ionic conductivities of 0.5 M LiTFSI in different ionic liquids.[a]

IL electrolyte	σ_0/S cm^{-1}	B/K	T_0/K
0.5 M LiTFSI/[EMIm][TFSI]	0.23 ± 0.13	323 ± 131	214 ± 23
0.5 M LiTFSI/[ETMIm][TFSI]	0.70 ± 0.3	746 ± 133	179 ± 13
0.5 M LiTFSI/[DMBIm][TFSI]	1.20 ± 0.63	842 ± 175	166 ± 17

[a] Equation (1) ($\sigma = \sigma_0 \exp[-B/(T - T_0)]$) was used.

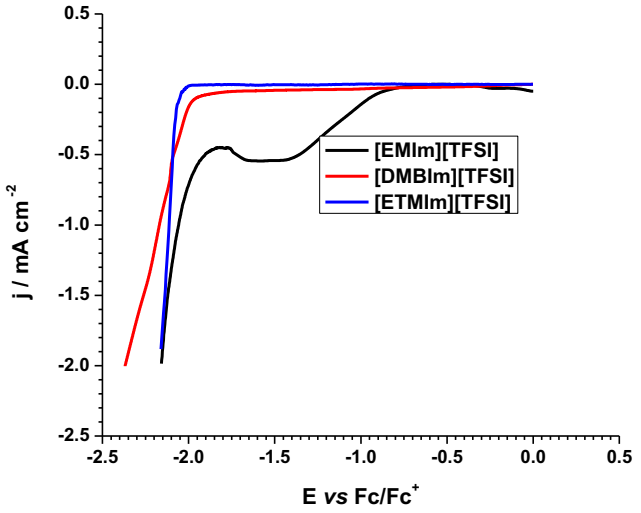

Fig. 3. Linear sweep voltammograms of pure ionic liquids on a Pt working electrode (surface area: 0.00196 cm^2) during the first cathodic scan from 0 to −3 V (versus ferrocene couple) at room temperature.

Li/Li^+ and the onset reduction potentials taken from Fig. 3, are tabulated in Table 3. First, the computed reduction potentials for the three ILs follow a trend of cathodic stability similar to those of the measured ones. Second, a good correlation between the LUMO level and those reduction potentials is apparent; that is, the higher the LUMO level, the more stable is the cation against reduction. The reductively stable cations of ETMIm and DMBIm can be attributed to the fact that the highly reducible hydrogen on the C-2 position of the imidazolium ring was replaced by the alkyl groups.

Fig. 4a and b shows the cyclic voltammograms (CVs) of the IL electrolytes of (a) 0.5 M LiTFSI/[ETMIm][TFSI] and (b) 0.5 M LiTFSI/[DMBIm][TFSI] measured on a platinum working electrode at the scan rate of 10 mV s^{-1}, respectively. A major lithium deposition is observed for both IL electrolytes during the cathodic scan; however, a major lithium stripping peak is observed for the 0.5 M LiTFSI/[ETMIm][TFSI] electrolyte, whereas major Li–Pt alloying peaks are observed for the 0.5 M LiTFSI/[DMBIm][TFSI] solution during the anodic scan. [4] It is observed that during the initial cathodic scan the nucleation overpotential is 50 mV for the [ETMIm][TFSI] solution while it is 300 mV for the [DMBIm][TFSI] solution. The difference in the overpotential can be partially explained by the slow ion diffusion in the more viscous [DMBIm][TFSI] solution (Table 1 for viscosity and Fig. 2 for ionic conductivity) [40,41]. However, it contradicts with the higher current density observed in the latter solution (Fig. 4b), which indicates that there are some side reactions contributing to the higher current of the latter. This might be due to the higher reactivity of the freshly deposited lithium [40], which quickly reacts with the ionic liquid and contributes to the observed higher current. This is supported by the apparent lower coulombic efficiency of DMBIm][TFSI] solution and the additional oxidation peak observed at 2.6 V *vs* Li/Li^+ during the immediate

Table 3
Comparison of properties of ionic liquids: The computed LUMO levels (eV), computed reduction potential *vs* Li^+/Li (V) at 298 K, and measured reduction potential *vs* Fc/Fc^+ (V).

IL	LUMO (eV)	Calculated reduction potential *vs* Li^+/Li (V)	Measured reduction potential *vs* Fc/Fc^+ (V)
[EMIm][TFSI]	−1.59	1.67	−0.83
[DMBIm][TFSI]	−1.41	1.44	−1.97
[ETMIm][TFSI]	−1.37	1.39	−2.05

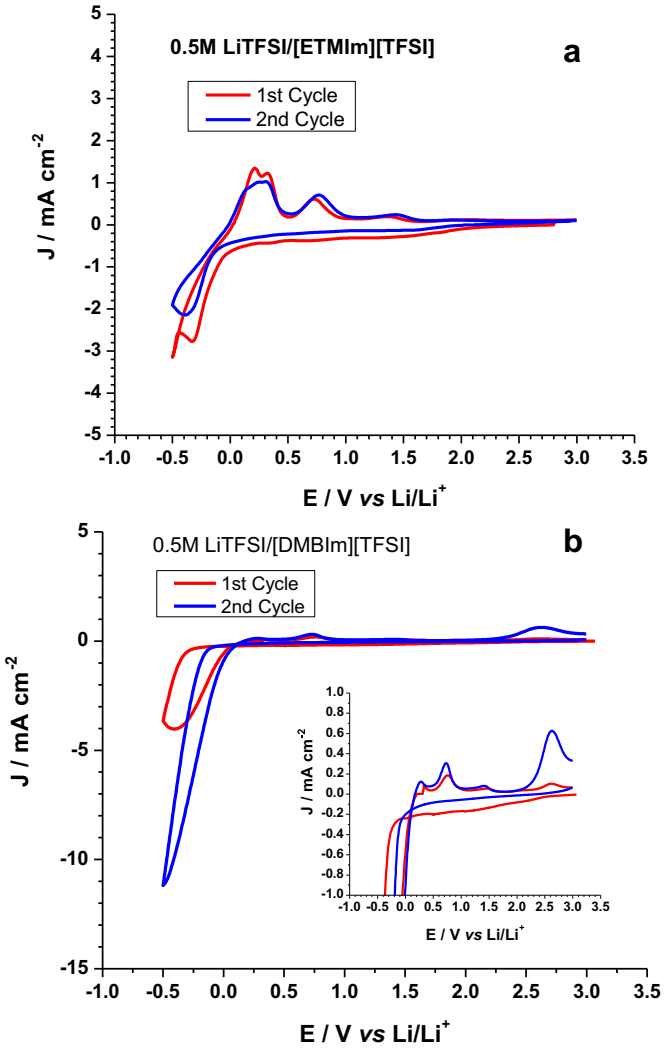

Fig. 4. Cyclic voltammograms of ionic liquid electrolytes of (a) 0.5 M LiTFSI/[ETMIm][TFSI] and (b) 0.5 M LiTFSI/[DMBIm][TFSI] on a Pt working electrode under a scan rate of 10 mV s^{-1} at room temperature (Li is used as both counter and reference electrode).

anodic scan (Fig. 4b). Furthermore, the higher lithium deposition current density in the second CV cycle corresponds well with a higher oxidation current peak [inlet of Fig. 4b]. The above facts indicate that not only [DMBIm][TFSI] is more reactive toward lithium but also the resulting products cannot passivate the Pt electrode. As a comparison, for the [ETMIm][TFSI] solution the current density of the second cycle is lower than that of the first cycle (Fig. 4a), which clearly indicates that the Pt electrode is passivated by the reduction products of the ionic liquid [40]. Finally, it is noted in both Fig. 4a and the inlet of Fig. 4b that the onset reduction potentials are 2.10 V and 2.35 V for [ETMIm][TFSI] and [DMBIM][TFSI], respectively. This reduction order is consistent with that observed in Fig. 3 and that calculated in Table 1.

The nonflammability of IL electrolytes allows the possibility of using lithium metal as an anode in lithium batteries, which can offer significantly higher energy density than graphite-based lithium ion batteries. However, that possibility, to a large extent, depends on whether the IL electrolyte is stable against lithium electrodes or a stable SEI can be formed to prevent further reactions once it reacts with the lithium electrode. To test the stability, Li/Li symmetric cells were assembled with the two IL electrolytes, 0.5 M LiTFSI/[ETMIm][TFSI] and 0.5 M LiTFSI/[DMBIm][TFSI]; and their

impedance spectra were monitored with time, as shown in Fig. 5a and b, respectively. The typical impedance spectra for lithium electrodes consist of one superimposed semicircle at high frequency, which is the total interphasial resistance and charge transfer resistance resulting mainly from the SEI film formed on the surface of the lithium electrodes (R_{SEI}) [42]. The intercept at high frequency is the resistance of the bulk electrolyte (R_{bulk}), which remains nearly constant during the period of the storage test. Fig. 5c shows the evolutions of R_{SEI} with time for both cells, which increase quickly within the first few hours. However, for the cell of [ETMIm][TFSI] the increase of R_{SEI} becomes much slower after 10 h and it tends to be stabilized; whereas for the cell of [DMBIm][TFSI] the increase of R_{SEI} is only slowed down after 14 h and it further fluctuates with time. The above fact indicates that [ETMIm][TFSI] can quickly passivate the lithium electrode effectively, which prevents further reactions and results in smaller R_{SEI}. This is also consistent with that observed in Fig. 4 for the cyclic voltammetry results, i.e. the [ETMIm][TFSI] can effectively passivate the Pt electrode while [DMBIm][TFSI] cannot. Nonetheless, the overall smaller R_{SEI} for the cell of [ETMIm][TFSI] is beneficial for quicker ion transport through the interphase as well as into and out of the electrode during cycling.

3.4. Performance of Li||Graphite half-cells

Fig. 6a and b shows the first three charge–discharge cycles of the Li||graphite half-cells based on 0.5 M LiTFSI/[DMBIm][TFSI] and 0.5 M LiTFSI/[ETMIm][TFSI], respectively, under a current density of C/20 at room temperature. The initial discharge (intercalation) and charge (de-intercalation) capacities for the cell of [DMBIm][TFSI] are 408 mA h g^{-1} and 254 mA h g^{-1}, respectively, resulting in a coulombic efficiency of 62%. As a comparison, the discharge and charge capacities for the cell of [ETMIm][TFSI] are 440 mA h g^{-1} and 256 mA h g^{-1}, respectively, resulting in a coulombic efficiency of only 58%. The lower coulombic efficiency in the latter cell is correlated with the longer plateau in the voltage range of 0.7 to 0.4 V, which indicates that there is a severe imidazolium cation intercalation [43]. This result indicates that the bicyclic structure still cannot prevent the imidazolium cation intercalation. Nonetheless, the cation intercalation doesn't cause graphite exfoliation. It is noted that the coulombic efficiency is quickly improved to 90 and 95% in the second and third cycles, respectively. More important, the charge capacities of the second and third cycle are kept at 251 and 261 mA h g^{-1}, respectively. As a comparison, although higher coulombic efficiencies are obtained for the cell of DMBIm][TFSI] in the first three cycles (see the legend of Fig. 6a), the charge capacities of the second and third cycle decrease to 197 and 164 mA h g^{-1}, respectively. The poor capacity retention of the cell of [DMBIm][TFSI] under C/20 becomes worse when the current density is increased to C/10. As shown in Fig. 6c, the capacity under C/10 not only drops more than half of that under C/20 but also decreases quickly with cycling; i.e. the initial capacity of 64 mA h g^{-1} drops to 10 mA h g^{-1} after 30 cycles. It is encouraging to note that the cell of [ETMIm][TFSI] exhibits an initial capacity of 73 mA h g^{-1} under a current rate of C/10, which slowly decreases to 66 mA h g^{-1} after 30 cycles. The lower capacity both at C/20 and C/10 than the theoretical capacity of graphite is mainly due to the high viscosity of the IL [38]. Nonetheless, the stable cycling performance of [ETMIm][TFSI] compared with that of [DMBIm][TFSI] can be attributed only to the more stable structure and good SEI

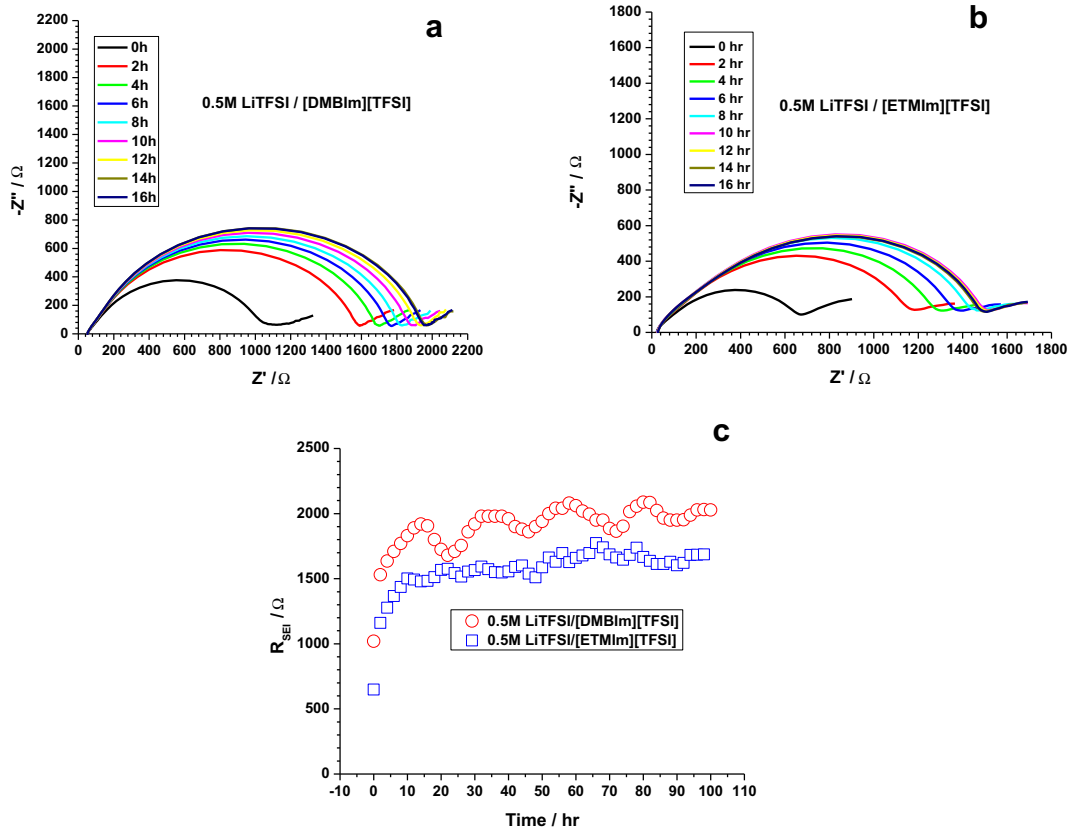

Fig. 5. The time dependence of electrochemical impedance spectra of the symmetric Li cell based on ionic liquid electrolyte (a) 0.5 M LiTFSI/[DMBIm][TFSI] and (b) 0.5 M LITFSI/[ETMIm][TFSI] at room temperature; (c) comparison of the time dependence of the solid electrolyte interphase (SEI) resistance of the two ionic liquid electrolytes at room temperature.

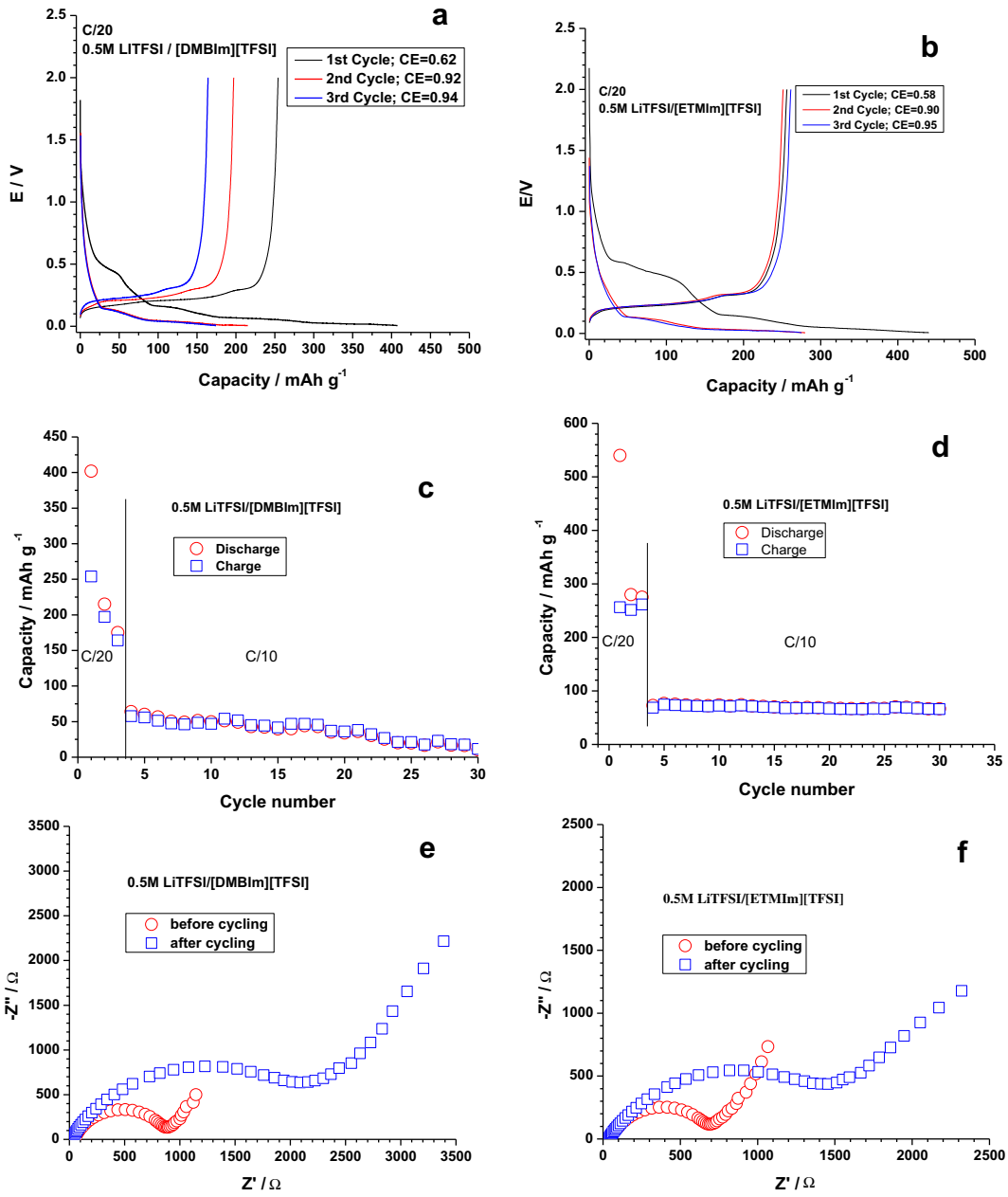

Fig. 6. Charge/discharge profile of the Li||graphite half-cells based on (a) 0.5 M LiTFSI/[DMBIm][TFSI] and (b) 0.5 M LiTFSI/[ETMIm][TFSI]; cycling performance of the Li||graphite half-cells based on (c) 0.5 M LiTFSI/[DMBIm][TFSI] and (d) 0.5 M LiTFSI/[ETMIm][TFSI] under different current densities at room temperature; impedance of the Li||graphite half-cells based on (e) 0.5 M LiTFSI/[DMBIm][TFSI] and (f) 0.5 M LiTFSI/[ETMIm][TFSI] before and after cycling at room temperature.

formation of the former, considering that the only difference between the two ILs is the cation structure. To confirm this conclusion, impedance spectra of the two cells were compared before and after cycling. Fig. 6e and f shows the cell impedance of [DMBIm][TFSI] and [ETMIm][TFSI], respectively. As mentioned previously regarding the impedance of Li||Li cells, the total interphasial impedance (R_{SEI}) can be easily obtained from the superimposed semicircle in the high frequency range. It is noted from Fig. 6e and f that after 30 cycles, the R_{SEI} of [DMBIm][TFSI] increases from 888 Ω before cycling to 2250 Ω after cycling, whereas the R_{SEI} of [ETMIm][TFSI] increases from 672 Ω before cycling to 1450 Ω after cycling. The increased R_{SEI} with cycling is mainly due to the reaction and reduction of the IL electrolyte on the surface of the lithium and graphite electrodes, respectively. This is especially true for the lithium metal freshly formed within each cycle, whose reaction with the ionic liquid has been proved to be responsible for the increase in impedance during repeated charge/discharge cycling [44]. The impedance data in Fig. 6 is also consistent with the result of CV and Li||Li impedance data that [ETMIm][TFSI] is better than [DMBIm][TFSI] for passivating the lithium electrode. Comparatively, the much higher R_{SEI} of the former cell is well accounted for by its relatively poor cell performance under the same cycling conditions.

To reduce the viscosity of the IL electrolyte and increase the cell capacity, as well as improve the cycling performance, fresh coin cells were built using the two IL electrolytes and cycled at 50 °C under different current rates. Fig. 7a and b shows the cycling performance of the cells of [DMBIm][TFSI] and [ETMIm][TFSI],

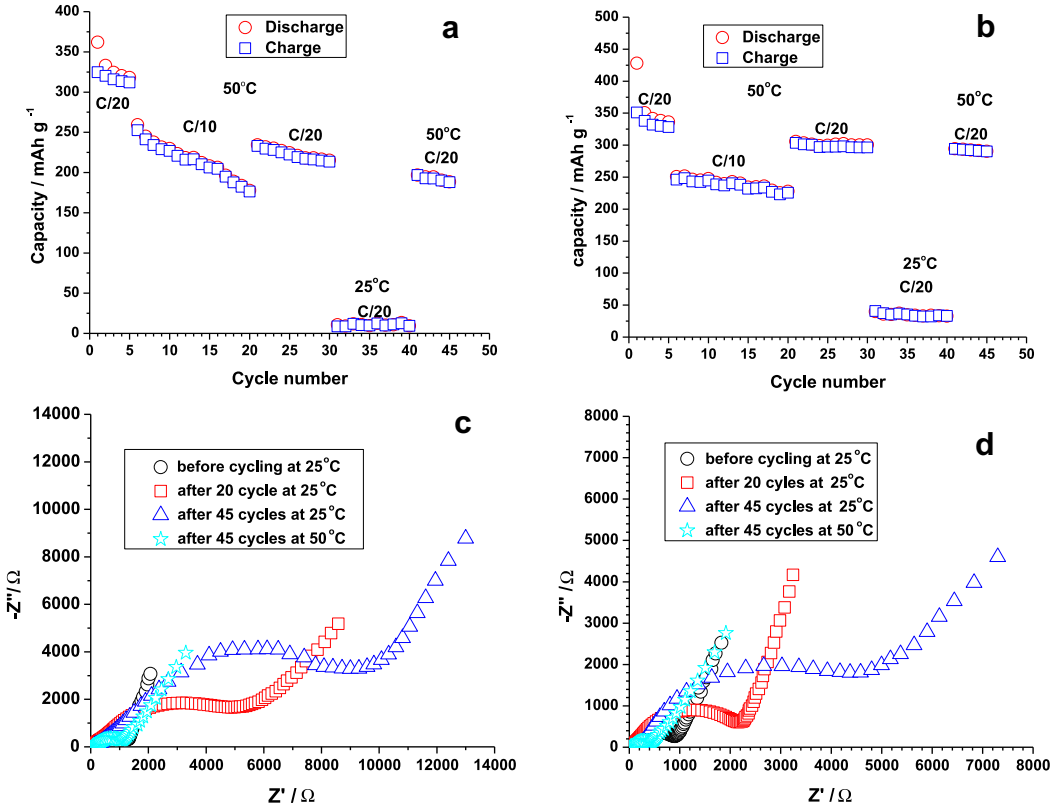

Fig. 7. Cycling performance of the Li||graphite half-cells based on a) 0.5 M LiTFSI/[DMBIm][TFSI] and b) 0.5 M LiTFSI/[ETMIm][TFSI] under different current densities at varied temperatures; impedance of the Li||graphite half-cells based on c) 0.5 M LiTFSI/[DMBIm][TFSI] and d) 0.5 M LiTFSI/[ETMIm][TFSI] (conditions are identified in the figure caption).

respectively. Indeed, with reduced viscosity and under a current rate of C/20, the initial discharge/charge capacities are increased to 362/324.6 mA h g^{-1} for the cell of [DMBIm][TFSI] and 428.1/350.9 mA h g^{-1} for the cell of [ETMIm][TFSI] cell, respectively. It is also noted that the coulombic efficiencies at 50 °C are much higher than those at 25 °C, that is, 89.7% for the cell of [DMBIm][TFSI] and 82.0% for the cell of [ETMIm][TFSI]. But as observed at 25 °C, for both cells the coulombic efficiencies quickly improve to above 98% within five cycles. When the current is increased to C/10, the initial capacities of both cells drop to around 250 mA h g^{-1}. However, the capacity for the cell of [DMBIm][TFSI] quickly decreases to 177 mA h g^{-1}, whereas the capacity for the cell of [ETMIm][TFSI] maintains at 228 mA h g^{-1} after 20 cycles. In addition, when the current is switched back to C/20, the capacity of [DMBIm][TFSI] recovers to 234 mA h g^{-1} and then quickly decreases to 215 mA h g^{-1} at the 30th cycle (Fig. 7a). By comparison, the capacity of [ETMIm][TFSI] increases to 306 mA h g^{-1} when the current is reduced to C/20 and gradually drops to 300 mA h g^{-1} at the 30th cycle (Fig. 7b). Furthermore, when the current rate is maintained at C/20 and the temperature drops from 50 to 25 °C, the capacities of both cells decrease significantly; for example, the capacity of [DMBIm][TFSI] is only around 10 mA h g^{-1} (Fig. 7a) and that of [ETMIm][TFSI] is around 35 mA h g^{-1} (Fig. 7b). However, once the temperature is increased again to 50 °C, the capacity of [DMBIm][TFSI] immediately recovers to 197 mA h g^{-1} and that of [ETMIm][TFSI] recovers to 295 mA h g^{-1}, from which they gradually decay with cycling.

The cell impedance (R_{SEI}) was monitored during cell cycling, which are shown in Fig. 7c and d for the R_{SEI} of DMBIm][TFSI] and [ETMIm][TFSI], respectively. The initial difference in R_{SEI} is small—1260 Ω for the cell of [DMBIm][TFSI] and 900 Ω for the cell of [ETMIm][TFSI]. However, R_{SEI} quickly increases to 5200 Ω after 20 cycles and 9300 Ω after 45 cycles for the cell of [DMBIm][TFSI], whereas it only moderately increases to 2200 Ω after 20 cycles and 4600 Ω after 45 cycles for the cell of [ETMIm][TFSI]. On the one hand, the combined huge interphasial and charge transfer impedance directly results in lower cell capacity for both cells at 25 °C under a current rate of C/20 (cycle 30–40, Fig. 7a and b). On the other hand, the significantly reduced cell impedances at 50 °C—1050 Ω for the cell of [DMBIm][TFSI] and 435 Ω for the cell of [ETMIm][TFSI] after cycling—which are only around a tenth of those at 25 °C, keep the cells functioning well at 50 °C.

It can be seen from these results that although it is beneficial to test lithium ion batteries based on IL electrolytes at 50 °C, it unavoidably accelerates the reaction of the IL electrolyte with lithium metal, which contributes to the buildup of the SEI layer and the increase in R_{SEI} [44]. This effect is evidenced by the larger R_{SEI} measured at 50 °C than at 25 °C after a similar number of cycles under the same cycling conditions (Fig. 6e and f *vs* Fig. 7c and d). It might be beneficial to use additives for the sole purpose of SEI formation for the IL electrolytes [38].

4. Conclusion

In this work, the ILs [ETMIm][TFSI], [DMBIm][TFSI], and [EMIm][TFSI] were tested as electrolytes for lithium ion batteries with the addition of 0.5 M LiTFSI as the lithium salt. The bicyclic structure of [ETMIm][TFSI] not only increases the reduction stability of the pure IL but also improves the electrochemical performance of the electrolyte in Li||graphite cells via formation of a relatively stable SEI layer. Generally, higher cell capacities are achieved at 50 °C than at 25 °C, facilitated by the reduced viscosity and better penetration of the IL electrolytes within the electrode and faster ion transport through the interphase as well as into and out of the electrodes.

However, the bicyclic structure unavoidably accelerates the reaction of the lithium electrode with the IL electrolytes at 50 °C compared with 25 °C, as is evidenced by the higher interphasial impedance of the cell cycled at 50 °C than at 25 °C under a similar number of cycles and cycling conditions. Nevertheless, the good compatibility with graphite electrode and better cycling performance of [ETMIm][TFSI], without using additive is remarkable, and it is a promising electrolyte for lithium ion battery applications.

Acknowledgments

This research was supported by the U.S. Department of Energy's Office of Basic Energy Science, Division of Materials Sciences and Engineering. J.R.B and H.M.L were supported by the U.S. Department of Energy, the Office of Nuclear Physics. C.L, N.S, J.R.B, and B.K.G acknowledge the Oak Ridge Associated Universities (ORAU) for postdoctoral fellowship.

References

[1] J. Sun, D.R. MacFarlane, M. Forsyth, Ionics 3 (1997) 356.
[2] M. Armand, F. Endres, D.R. MacFarlane, H. Ohno, B. Scrosati, Nat. Mater. 8 (2009) 621.
[3] M. Galinski, A. Lewandowski, I. Stepniak, Electrochim. Acta 51 (2006) 5567.
[4] H. Matsumoto, H. Sakaebe, K. Tatsumi, J. Power Sources 146 (2005) 45.
[5] P.C. Howlett, D.R. MacFarlane, A.F. Hollenkamp, Electrochem. Solid-State Lett. 7 (2004) A97.
[6] C. Sirisopanaporn, A. Fernicola, B. Scrosati, J. Power Sources 186 (2009) 490.
[7] E. Markevich, V. Baranchugov, G. Salitra, D. Aurbach, M.A. Schmidt, J. Electrochem. Soc. 155 (2008) A132.
[8] V. Baranchugov, E. Markevich, G. Salitra, D. Aurbach, G. Semrau, M.A. Schmidt, J. Electrochem. Soc. 155 (2008) A217.
[9] E. Markevich, V. Baranchugov, D. Aubach, Electrochem. Commun. 8 (2006) 1331.
[10] H. Sakaebe, H. Matsumoto, K. Tatsumi, Electrochim. Acta 53 (2007) 1048.
[11] H. Sakaebe, H. Matsumoto, Electrochem. Commun. 5 (2003) 594.
[12] T. Sato, T. Maruo, S. Marukane, K. Takagi, J. Power Sources 138 (2004) 253.
[13] H. Matsumoto, M. Yanagida, K. Tanimoto, M. Normura, Y. Kitagawa, Y. Miyazaki, Chem. Lett. (2000) 922.
[14] A. Fernicola, F. Croce, B. Scrosati, T. Watanabe, H. Ohno, J. Power Sources 174 (2007) 342.
[15] H. Sakaebe, H. Matsumoto, K. Tatsumi, J. Power Sources 146 (2005) 693.
[16] M. Ishikawa, T. Sugimoto, M. Kikuta, E. Ishiko, M. Kono, J. Power Sources 162 (2006) 658.
[17] J. Xu, J. Yang, Y. Nulu, J. Wang, Z. Zhang, J. Power Sources 160 (2006) 621.
[18] C.M. Lang, P.A. Kohl, J. Electrochem. Soc. 154 (2007) F106.
[19] H. Zheng, B. Li, Y. Fu, T. Abe, Z. Ogumi, Electrochim. Acta 52 (2006) 1556.
[20] J.H. Shin, P. Basak, J.B. Kerr, E. Cairns, J. Electrochim. Acta 54 (2008) 410.
[21] J.Y. Mun, Y.S. Jung, T. Yim, H.Y. Lee, H.J. Kim, Y.G. Kim, S.M. Oh, J. Power Sources 194 (2009) 1068.
[22] G.B. Appetecchi, M. Montanino, A. Balducci, S.F. Lux, J. Power Sources 192 (2009) 599.
[23] S.F. Lux, M. Schmuck, G.B. Appetecchi, S. Passerini, M. Winter, A. Balducci, J. Power Sources 192 (2009) 606.
[24] D.R. MacFarlane, P. Meakin, J. Sun, N. Amini, M. Forsyth, J. Phys. Chem. B. 103 (1999) 4164.
[25] P.C. Howlett, D.R. MacFarlane, A.F. Hollenkamp, J. Power Sources 114 (2003) 277.
[26] S. Seki, Y. Kokayashi, H. Miyashiro, Y. Ohno, A. Usami, Y. Mita, N. Kihira, M. Watanabe, N. Terada, J. Phys. Chem. B. 110 (2006) 10228.
[27] R.S. Brown, H. Slebocka-Tilk, J.M. Buschek, J.G. Ulant, J. Am. Chem. Soc. 106 (1984) 5979.
[28] H.C. Kan, M.C. Tseng, Y.H. Chu, Tetrahedron 63 (2007) 1644.
[29] M.C. Tseng, M.J. Tseng, Y.H. Chu, Chem. Commun. 48 (2009) 7503.
[30] T.E. Sutto, P.C. Trulove, H.C. De Long, Electrochem. Solid-State Lett. 6 (2003) A50.
[31] C. Liao, N. Shao, K.S. Han, X.G. Sun, D.E. Jiang, S. Dai, Phys. Chem. Chem. Phys. 13 (2011) 21503.
[32] A.D. Becke, J. Chem. Phys. 98 (1993) 5648.
[33] C.T. Lee, W.T. Yang, R.G. Parr, Phys. Rev. B 37 (1988) 785.
[34] N. Shao, X.G. Sun, S. Dai, D.E. Jiang, J. Phys. Chem. B. 115 (2011) 12120.
[35] N. Shao, X.G. Sun, S. Dai, D.E. Jiang, J. Phys. Chem. B. 116 (2012) 3235.
[36] M.J. Frisch, G.W. Trucks, H.B. Schlegel, G.E. Scuseria, M.A. Robb, J.R. Cheeseman, G. Scalmani, V. Barone, B. Mennucci, G.A. Petersson, H. Nakatsuji, M. Caricato, X. Li, H.P. Hratchian, A.F. Izmaylov, J. Bloino, G. Zheng, J.L. Sonnenberg, M. Hada, M. Ehara, K. Toyota, R. Fukuda, J. Hasegawa, M. Ishida, T. Nakajima, Y. Honda, O. Kitao, H. Nakai, T. Vreven, J.A. Montgomery Jr., J.E. Peralta, F. Ogliaro, M. Bearpark, J.J. Heyd, E. Brothers, K.N. Kudin, V.N. Staroverov, R. Kobayashi, J. Normand, K. Raghavachari, A. Rendell, J.C. Burant, S.S. Iyengar, J. Tomasi, M. Cossi, N. Rega, N.J. Millam, M. Klene, J.E. Knox, J.B. Cross, V. Bakken, C. Adamo, J. Jaramillo, R. Gomperts, R.E. Stratmann, O. Yazyev, A.J. Austin, R. Cammi, C. Pomelli, J.W. Ochterski, R.L. Martin, K. Morokuma, V.G. Zakrzewski, G.A. Voth, P. Salvador, J.J. Dannenberg, S. Dapprich, A.D. Daniels, Ö. Farkas, J.B. Foresman, J.V. Ortiz, J. Cioslowski, D.J. Fox, Gaussian 09, Gaussian, Inc., Wallingford CT, 2009.
[37] J. Reiter, M. Nadherna, R. Dominiko, J. Power Sources 205 (2012) 402.
[38] X.G. Sun, S. Dai, Electrochim. Acta 55 (2010) 4618.
[39] H. Tokuda, K. Ishii, M.A.B.H. Susan, S. Tsuzuki, K. Hayamizu, M. Watanabe, J. Phys. Chem. B. 110 (2006) 19593.
[40] J. Xu, G.C. Farrington, Solid State Ionics 74 (1994) 125.
[41] R. Wibowo, S.E.W. Jone, R.G. Compton, J. Phys. Chem. B. 113 (2009) 12293.
[42] D. Aurbach, J. Power Sources 89 (2000) 206.
[43] H.H. Zheng, K. Jiang, T. Abe, Z. Ogumi, Carbon 44 (2006) 203.
[44] P. Reale, A. Fernicola, B. Scrosati, J. Power Sources 194 (2009) 182.